Developing a Tracking-Based Dynamic Flash Yellow Arrow Strategy for Permissive Left-Turn Vehicles to Improve Pedestrian Safety at Intersections

Farzana Rahman Chowdhury, Ph.D., S.M.ASCE[1]; Peirong "Slade" Wang, S.M.ASCE[2]; and Pengfei "Taylor" Li, Ph.D., P.Eng., M.ASCE[3]

Abstract: Recent data have shown that pedestrian fatalities have increased by 44% from 2010 to 2019. In 2019, 6,590 pedestrians died of traffic crashes, and 20% occurred at intersections, the highest in 30 years. These saddening facts, unfortunately, suggest that walking or biking is even less safe today although driving is safer thanks to numerous efforts in vehicular technologies. Smart transportation is successful only if it provides equitable safety for all road users. Flash yellow arrow (FYA) is a left-turn strategy at signalized intersections in North America. It allows left-turn vehicles to cross when the gaps of opposing through-traffic are perceived as safe. But it cannot separate concurrent crossing pedestrians and left-turn vehicles. To address this issue, a novel dynamic flash yellow arrow (D-FYA) solution is developed using the light detection and ranging (LiDAR)-based tracking technique. It can address the safety concerns in the FYA while recovering the permissive left-turn capacity after the concurrent pedestrians are cleared. Depending on the pedestrian volumes, the corresponding FYA with each cycle will either start as scheduled, be postponed, or be canceled within each cycle. The proposed D-FYA was deployed at an intersection next to the campus of the University of Texas at Arlington, and its real-time D-FYA decisions in the field were verified over 100 traffic signal cycles through simultaneous observation in the field. The proposed D-FYA solution was further evaluated within a traffic signal simulation platform to compare its mobility performance with another two permissive left-turn strategies: (1) protected + permissive left turn (PPLT), and (2) PPLT with minus-pedestrian phase. The experiment results revealed the D-FYA is accurate and adaptive compared with the other two permissive left-turn strategies. **DOI: 10.1061/JTEPBS.TEENG-7457.**

Author keywords: Traffic safety; Vision zero; Traffic signal operations; Flash yellow arrow (FYA); Traffic signal simulation; Intersection capacity analysis.

Introduction

The surface transportation system is experiencing rapid changes today. Not only is travel demand increasing, but also the travel modes are diversified. People have more choices for travel other than traditional vehicles, from self-driving cars to e-scooters. There are many initiatives toward smart infrastructure and intelligent vehicles at federal, state, and municipal levels to accommodate these new trends. Although these efforts are modernizing the transportation system, issues of equitable safety are surfacing. Pedestrian safety is a critical prerequisite to promoting walkability in cities. In the 21st century, transportation developments in the US are largely focused on making the driver's experience as expedient and frictionless as possible, with little attention paid to the demands of pedestrians or technical advancements for pedestrian safety (Gutfreund 2004; Levinson and Krizek 2007).

Even more urgent is that pedestrian fatalities are taking up an increasing percentage of total traffic fatalities although overall traffic fatalities have been decreasing. According to a National Highway Traffic Safety Administration (NSHTA) report, pedestrian fatalities have increased by 44% from 2010 to 2019. In 2019, 6,590 pedestrians died in traffic crashes, the highest in 30 years (Ziebarth 2020). Unfortunately, these saddening facts suggest that walking or biking on the street is less safe today. Although most efforts have been devoted to improving mobility and safety for vehicles, the safety of pedestrians on roads is left far behind.

Inductive loop sensors have been used to detect and facilitate motor vehicles since the 1960s (Klein et al. 2006), but this technology is by nature difficult to detect pedestrians due to variations in their walk/roll patterns and grouping arrangements as well as the sensor's limitations in a variety of environmental conditions, such as brightness and darkness, high and low temperatures, rain, ice, and snow. Smart transportation is smart only if it provides equitable safety for all road users. In particular, vulnerable pedestrians should be paid the most attention. There are many aspects of pedestrian safety improvement from the perspective of technology. The efforts can be categorized into four levels, as shown in Fig. 1.

Specifically, these four levels are as follows:

- Level 1: Observe pedestrian behaviors. Pedestrian data are mostly composed of counts today. Although there are available databases to store pedestrian delays and crashes, they are less common than pedestrian volumes. Although the pedestrian counts reflect the needs for pedestrian facilities, they do not necessarily represent pedestrian safety. As such, it is necessary to

[1]Dept. of Civil Engineering, Univ. of Texas at Arlington, Arlington, TX 76019. Email: farzana.chowdhury@mavs.uta.edu

[2]Ph.D. Student, Dept. of Civil Engineering, Univ. of Texas at Arlington, Arlington, TX 76019. ORCID: https://orcid.org/0000-0002-9636-7047. Email: Peirong.wang@mavs.uta.edu

[3]Assistant Professor, Dept. of Civil Engineering, Univ. of Texas at Arlington, Arlington, TX 76019 (corresponding author). ORCID: https://orcid.org/0000-0002-3833-5354. Email: Taylor.Li@uta.edu

Note. This manuscript was submitted on March 29, 2022; approved on November 18, 2022; published online on January 31, 2023. Discussion period open until June 30, 2023; separate discussions must be submitted for individual papers. This paper is part of the ***Journal of Transportation Engineering, Part A: Systems***, © ASCE, ISSN 2473-2907.

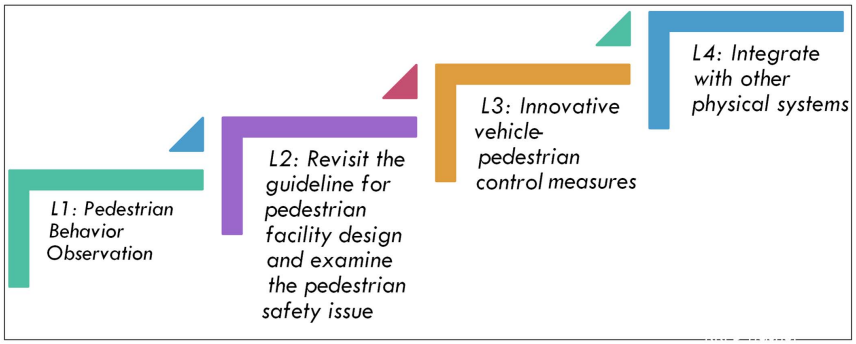

Fig. 1. Four levels of pedestrian safety improvement.

collect pedestrian behavioral data for better-informed decision makings toward pedestrian safety improvement.

- Level 2: Revisit the design guideline for pedestrian facility design. With more pedestrian behavioral data, it becomes possible to inspect the effectiveness of existing pedestrian facilities and validate the current design guideline. Level 2 measures primarily aim at planning.
- Level 3: Novel control measures to improve pedestrian safety. This level involves real-time pedestrian behavioral data collection and real-time pedestrian protection, such as reducing pedestrian conflicts with vehicles. Level-3 measures are primarily aimed at operations. The proposed dynamic flash yellow arrow (D-FYA) system belongs to this level.
- Level 4: Integrate with other physical systems. At this level, multiple physical systems will be integrated to further protect pedestrians. For instance, the D-FYA system can be coupled with a lighting system to provide supplemental lights for crossing pedestrians at night. Level-4 solutions are rare today, but those novel solutions may be highly effective to protect pedestrians.

In this paper, a dynamic flash yellow arrow mechanism is proposed based on a state-of-the-art light detection and ranging (LiDAR) tracking system to fully protect concurrent crossing pedestrians from permissive left-turn vehicles. In category, it falls into the Level-3 pedestrian protection activities as defined previously. The major benefit of this new D-FYA method is to separate the concurrent crossing pedestrians more effectively from permissive left-turn vehicles while using all safe permissive left-turn capacities. This feature is especially beneficial when a phase duration is much longer than the required pedestrian crossing time.

Literature Review

After an extensive search, it can be concluded that most related literature focused on pedestrian detection techniques, but few are related to applying tracking technologies to real-time traffic signal operations to improve pedestrian safety. Therefore, this literature review focuses on pedestrian detection technology. In most literature, pedestrians and bicyclists are often stated together, referred to as pedestrian and bicyclist detection (PBD). A rich body of literature on such sensing technologies is available as well, such as video processing, infrared cameras, radar, and LiDAR sensing technologies. The back-end algorithms of such sensing technologies are mostly based on clustering and machine learning techniques. This literature review focuses on two aspects: (1) pedestrian detection techniques; and (2) the application of these techniques.

Pedestrian Detection Using Cameras

Pedestrian detection using cameras is based on the subtraction of the moving objects (i.e., pedestrians) from the stationary background. Using video-based pedestrian detections, Kilambi et al. (2008) adopted the Gaussian density method to estimate the number of people in a group. The proposed projection method could find each blob area obtained from foreground segmentation in the world coordinate using camera calibration information. Although the method can lower the issues generated due to the moving objects of different heights (i.e., vehicles) other than the human height, it cannot give the crowd's motion trajectory information. Later, Yoshinaga et al. (2010) used a blob descriptor to find the crowd size. Although the pixel values in this model were observed in the massive frames, the developed neural network could not always give the correct estimation because the image contains a high volume of information.

Chan et al. (2018) developed a modified algorithm for surveillance video technology. The database used to prove the concept was a 1-h video recorded by a stationary digital camcorder. Chan and Vasconcelos (2009) further used Bayesian Poisson regression for counting the crowd size. Bhuvaneshwar and Mirchandani (2004) proposed a systematic approach for counting and detecting pedestrians at an intersection using a video camera. They also proposed a shadow removal algorithm for the detection and removal of the object from the image frames. The proposed system can report a general idea about the number and location of pedestrians at the intersection. Nonetheless, even though video-based pedestrian detection techniques can identify the crowd size without the location information of pedestrians, the accuracy is highly sensitive to the position, and installation angle of cameras, creating large errors. Because of these reported issues in practice, using video detection for large-scale pedestrians is limited (Li et al. 2012).

Pedestrian Detection Using Thermal Camera/Passive Infrared

Pedestrians can also be detected using a thermal camera and passive infrared. Both thermal cameras and passive infrared (PIR) sensors use passive detection of infrared light. However, when thermal images are used for pedestrian detection, the actual size and color information cannot be accurately collected. Moreover, weather changes also impact the outcome because the thermal sensors also visualize temperature radiation from the objects in the images. John et al. (2017) calibrated and analyzed the images from a thermal camera [forward looking infrared (FLIR) far-infrared camera] and visible cameras [imaging development systems (IDS) visible camera] to perform pedestrian detection (John et al. 2017). Baek et al. (2017) proposed a thermal position intensity histogram (TPIHOG) for pedestrian detection at night using a thermal camera.

Kim (2019) developed a multistage cascade learning device for pedestrian detection at night time or in a location of lower light. In this approach, the author estimated the distance between the detected pedestrian area and the infrared camera location with the information on the position of a pedestrian who was detected in the real-world environment in the two-dimensional (2D) thermal image. Most recently, Khalifa et al. (2020) took a compensation method to detect pedestrians from a moving camera, a traditionally challenge task due to the difficulty of background subtraction.

Pedestrian Detection Using Active Infrared

Active infrared sensors are another method of pedestrian detection. Those sensors effuse an infrared light beam to the receiver located across a pedestrian path. If any pedestrian enters that path, the beam is blocked, and thus one pedestrian count is added to the record. However, the limitation of active infrared detection is that it cannot identify pedestrians and bicyclists separately. Also, the range of detection locations is very small. Because of its limitations, active infrared is generally used for pedestrian-only trails, where the pedestrian path is constrained and classification is not necessary, as summarized by Kothuri et al. (2017). Khalifa et al. (2020) developed a novel compensation method to detect pedestrians from a moving camera. Islam et al. (2021) took the Kalman filter and deep learning techniques to fuse camera and LiDAR data for pedestrian detection (Islam et al. 2021). Yan et al. (2021) took the logic minimization method to detect pedestrians through multiple simultaneous cameras. Yang et al. (2021) developed a multitask region-based convolutional neural network (R-CNN) model to detect pedestrians and estimate the distance at night.

Detecting Using Radar Sensor

Radio detection and ranging (radar) is an active sensor with a wide span of usable wavelengths (100 m to 4 mm). Because of the longer wavelength, it can cover more objects. However, longer wavelengths produce lower-resolution sensor data. Manston (2011) utilized radar advanced driver assistance system (ADAS) features at certain pedestrian user friendly intelligent intersection (PUFFIN) crossings within test locations in order to detect pedestrians in motion within the crosswalk. When necessary, a dual antenna system can provide a curbside detection zone and a crosswalk detection zone. Limitations of radar include susceptibility to error from rainfall, although a 13-GHz radar has improved upon this limitation from previous 24-GHz models.

Pedestrian Detection Using LiDAR Sensor

LiDAR sensors are an emerging sensing solution. In transportation, LiDAR sensors were initially designed for autonomous vehicles to identify the surrounding objects. Although the application of LiDAR in transportation is mostly focused on autonomous vehicles, more and more LiDAR manufacturers have entered the area of infrastructure. With some natural physical advantages, LiDAR sensors are used to detect and trace pedestrians. Zhao and Shibasaki (2005) proposed a pedestrian tracking approach using multiple single-line LiDAR sensors. In this approach, real-time pedestrian behavioral data from a wide area were collected through a 360° spinning LiDAR, and then moving objects were extracted. They used the Kalman filter for developing a tracking algorithm to identify pedestrian trajectories.

Later, Zhao et al. (2011) applied a network of horizontal LiDAR sensors to monitor vehicle and pedestrian movement entering a large crowded intersection. They used data clustering techniques in an integrated special and temporal data association framework to find the moving object and motion trajectory at the intersection. However, the clustering was conducted manually without considering the same object entered into the database from different sensors. Moreover, a few critical parameters were estimated based on experience, making the study lack generality and weak adaptability. Zhao et al. (2019) later presented a systematic approach for tracking and detecting pedestrians at an intersection using infrastructure-based LiDAR sensors. The foremost step of the methodology was the background filtering of the collected data. After that, the objects were classified as pedestrians or vehicles.

Lv et al. (2019) developed a systematic approach to extract high-resolution traffic data from roadside LiDAR sensors to get and extract the trajectory information from the speed distance profile (SDP) of the road user to reduce vehicle–pedestrian conflicts. Wu et al. (2018) used high-resolution micro traffic data (HRMTD) from a LiDAR sensor based on the spatial distribution of laser points, which filtered both static and moving backgrounds efficiently. They used a background filtering method named three-dimensional density statistic filtering (3D-DSF) for efficiently separating static and dynamic backgrounds.

Combs et al. (2019) identified the range for pedestrian sensors. They estimated the maximum number of pedestrian fatalities that could be avoided if the system were converted into an automated vehicle environment. Grassi et al. (2011) developed a method based on data extraction and data fusion to detect pedestrians and classify them depending on their movement direction using both a LiDAR sensor and video camera. They classified the data without tracking or movement analysis. El Ansari et al. (2018) developed a hybrid pedestrian detection technology to identify both moving and static pedestrians by incorporating both 3D LiDAR data and vision sensors for data clustering.

Soundrapandiyan and Mouli (2015) and Tang et al. (2017) proposed an offline adaptive pedestrian detection using a neural network and collecting data from the sensor and video detection database. Soundrapandiyan and Mouli (2015) performed background modeling of the image collected from the thermal camera, and pedestrian detection was conducted by local adaptive thresholding using the parameter from the input image; on the other hand, Tang et al. (2017) used a controlled convolutional neural network (CCNN) architecture and modulating neural network (MNN) for detecting pedestrians in a location. CCNN works on adaptively generating a priority classifier, which is later dynamically adjusted by MNN (Tang et al. 2017). Readers are also recommended to read Tarko's (2019) study on using LiDAR to measure road safety.

Dynamic Flash Yellow Arrow Strategy Based on LiDAR-Based Pedestrian Tracking Technology

Along with red, yellow, and green steady arrow indicators, a flashing yellow arrow (FYA) is to indicate left-turn drivers to proceed if they can find acceptable gaps in the opposing traffic and no conflict with concurrent crossing pedestrians. FYA is an alternative permissive left-turn mechanism allowed by the latest manual on uniform traffic control devices (MUTCD 2009) to avoid the "yellow trap" in the "lead-lag" phasing sequence (Knodler et al. 2007). Compared with the traditional permissive left-turn method (circular green and dark left-arrow), FYAs are associated with the opposing green to ensure the opposing green is terminated when the left-turn vehicles are indicated with a steady yellow. FYAs have been widely adopted for permissive left-turn movements after the related research concluded that the FYA would improve traffic safety (Noyce et al. 2014).

Although a FYA resolves the yellow-trap issue for left-turn vehicles, it does not thoroughly consider the presence of concurrent crossing pedestrians. At this time, the standard FYA mechanism accounts for drivers' judgment to avoid crashes with pedestrians,

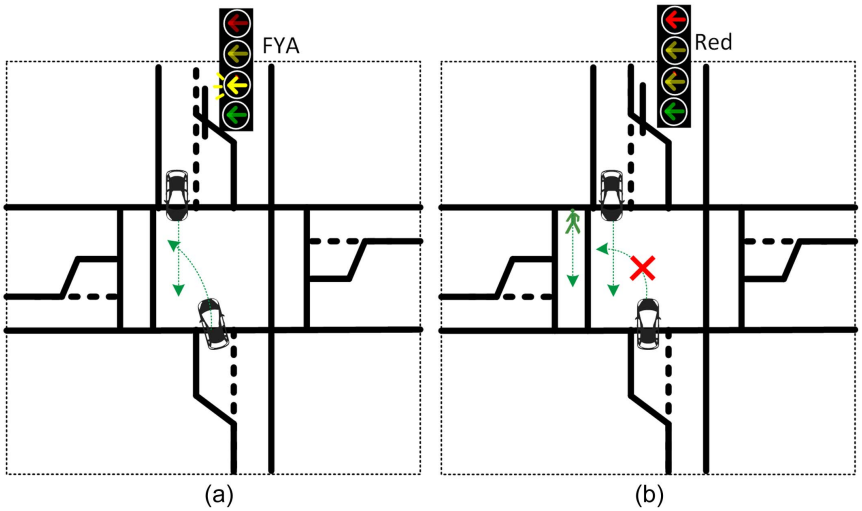

Fig. 2. Demonstration of FYA and minus pedestrian: (a) no ped call; and (b) with ped call.

which could become challenging in certain conditions like heavy traffic, blocked views, or dark conditions. As a result, pedestrian crashes reportedly increased at many locations after the implementation of FYA. To address this issue, agencies either turn the FYA off or adopt a special feature in some brands of traffic signal controllers, referred to as "minus pedestrian" (Q-Free America 2022). The idea of minus pedestrian is temporarily suppressing the FYA for a cycle if the corresponding pedestrian phase is called. Fig. 2 shows the concepts of FYA and the minus pedestrian.

Although the minus-pedestrian feature separates left-turn vehicles from concurrent crossing pedestrians, it also eliminates most permissive left-turn capability for that cycle, and it will not work if the pedestrian phase recall is placed. This mechanism often creates excessive left-turn queues during peak hours when both pedestrian volumes and left-turn vehicle volumes are high. A new dynamic FYA, or D-FYA, is designed in this paper based on a LiDAR-based pedestrian tracking system to address this issue. As shown in Fig. 3, concurrent crossing pedestrians have a conflict with left-turn vehicles only when they are within the so-called hazard zone.

Three-Zone Pedestrian Tracking with LiDAR Sensors

In reality, many pedestrians push the pedestrian buttons and then start to cross before the WALK sign starts or else they jaywalk (walk out of the designated areas while crossing). As a result, neither the pedestrian phase nor FYA suppressing will benefit from that cycle. In addition, the D-FYA can (and should) only protect those pedestrians who observe the traffic regulations. Overprotecting both legitimate and illegitimate crossing pedestrians will considerably interrupt traffic signal operations. To address these issues, a three-zone method is designed to filter and only track those legitimate crossing pedestrians (Fig. 3).

A pedestrian needs to enter the wait zone first and push the pedestrian button to be considered legitimate. The waiting zones (Zone 1) of each pedestrian phase are defined as far-end (Zone 1) and near-end (Zone 1') according to their relative locations to the left-turn vehicles. During WALK, if a pedestrian in Zone 1 and /or 1' enters the boundary zones (Zones 2 and 3), then this pedestrian is considered a legitimate pedestrian. If the same pedestrian reaches the other end, then this pedestrian crossing is considered finished. If the pedestrian button is pushed but no legitimate pedestrians enter the intersection, the pedestrian request is then considered void and ignored. The three-zone method will filter out those jaywalking pedestrians.

Dynamic Flash Yellow Arrow Based on Pedestrian Tracking

The D-FYA algorithm is elaborated as follows:

- When a traffic signal green phase starts: Reset all the FYAs as programmed initially.
- When this signal phase enters yellow and all-red: The proposed D-FYA algorithm will check the following items in sequence:
  Step 1: Check if this phase has a concurrent pedestrian phase. If yes, go to Step 2. If not, STOP
  Step 2: Check if the pedestrian button is pushed. If yes, go to Step 3. If not, STOP
  Step 3: Examine the existence of pedestrians in far-end and near-end waiting zones. There are two scenarios:
  a. No pedestrians are detected at either waiting zones, the D-FYA algorithm will keep the original FYA settings. Then go to Step 4.
  b. Pedestrians are detected at one or two waiting zones, then the D-FYA algorithm will suspend the programmed FYA temporarily. Then go to Step 4.
- When green or WALK starts, the D-FYA algorithm will check Step 4 to make the final decision on FYA for this cycle.
  Step 4: At this step, there are four possibilities for pedestrians to enter the intersection from two sides of the waiting zones.
  a. During the WALK time, if pedestrians from the far-end waiting zone (e.g., Zone 1 in Fig. 3) enter the intersection (e.g., Zone 2 in Fig. 3) but no pedestrians in the near-end waiting zone (e.g., Zone 1' in Fig. 3) enter (e.g., Zone 3 in Fig. 3). The FYA is suspended until all pedestrians have left the hazard zone (Fig. 3). Then, the FYA is re-activated until the current phase ends.
  b. During the WALK time, if pedestrians in the near-end waiting zone enter the intersection but no pedestrians in the far-end waiting zone enter, then the FYA is suspended until all near-end pedestrians reach the other side of the intersection (e.g., enter the boundary zone on the other side). Then the FYA is reactivated until the current phase ends.
  c. During the WALK time, if pedestrians enter the intersection from both sides, the FYA is suspended until all pedestrians reach the other side.
  d. During the WALK time, if no pedestrians enter from either side, the FYA is activated until the current phase ends.
  Step 4 is the final step of this algorithm for each phase.

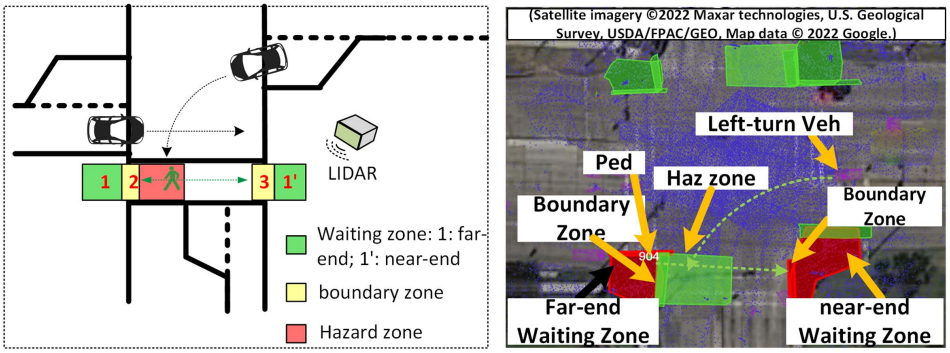

Fig. 3. Three-zone pedestrian detection method at intersections: (a) demonstration; and (b) zone settings in the field (satellite imagery ©2022 Maxar technologies, US Geological Survey, USDA/FPAC/GEO, Map data © 2022 Google).

The following points of discussion are highlighted:

- Decisions on FYA at Step 3 are temporary because a detected person in the waiting zones does not necessarily mean to cross, or a pedestrian may mistakenly push a pedestrian button. The final decision of keeping or suspending an FYA will be determined after the green/WALK starts.
- Activating FYA or not is made once and only once with each cycle to avoid confusing drivers and pedestrians. This condition is also known as the yellow trap.
- If a pedestrian jaywalks and gets out of the boundary zone when reaching the intersection's other side, LiDAR sensors will lose tracking it. The missing pedestrian will be allocated with the longest time walk time beyond which this person is considered to have crossed.
- The proposed D-FYA is particularly effective when the opposing green is much longer than the needed pedestrian crossing time. Once all pedestrians are cleared, the FYA is reactivated and can provide a significant permissive capacity for left-turn vehicles. By contrast, the current minus-pedestrian mechanism will unconditionally suppress the FYA all through the cycle even if no pedestrians cross or all pedestrians have crossed the intersection during a short period.

Analysis of Permissive Left-Turn Capacity under D-FYA

Although the D-FYA's safety benefits are obvious as opposed to the standard FYA (not separate left-turn vehicles and concurrent pedestrians systematically), it is important to ensure that the D-FYA will not interrupt traffic mobility too much. In this section, the changes to the permissive left capacity with the D-FYA as opposed to that with the protected + permissive left turn (PPLT) under different scenarios are analyzed. A traffic scenario in this context is composed of the duration of D-FYA, opposing through traffic volumes and the number of lanes, and the corresponding pedestrian volume. After the protected left-turn phase is over, the FYA will start together with the green for the opposing through traffic. The left-turn vehicles will begin to seek acceptable gaps to maneuver. While the queue of opposing traffic is being discharged, the left-turn vehicles cannot find the gaps due to the small headways. After the queuing vehicles are cleared, the left-turn vehicles will be able to find acceptable gaps to cross. If the permissive left-turn strategy is D-FYA, then the flash yellow arrow may start on time, be delayed, or even be canceled, depending on the presence of pedestrians. It can be formulated as follows (Table 1 presents the notation for the formulation).

As shown in Fig. 4, t_c is the time for clearing the queue of opposing through traffic and it can be calculated as follows:

Total arrivals during red and queue clearing time is $q \times (C - G + t_c)$.

Total departures during the queue clearing time is $s \times t_c$.

The total arrivals are equal to the total departures when the queue is cleared

$$q \times (C - G + t_c) = s \times t_c \tag{1}$$

Therefore

$$t_c = \frac{(C - G)}{\left(\frac{s}{q} - 1\right)} \tag{2}$$

Table 1. Traffic settings for the permissive left-turn capacity calculation

Item	Permissive LT			D-FYA ($n_p \leq 1$)			D-FYA ($n_p > 1$)		
Cycle length (s)	110	110	110	110	110	110	110	110	110
Opposing through green (s)	34	40	46	42	48	54	42	48	54
Base left-turn saturation flow rate (vehicles per hour per lane)	1,500	1,500	1,500	1,500	1,500	1,500	1,500	1,500	1,500
Volume of opposing through traffic (vehicles per hour per lane)	400	500	600	400	500	600	400	500	600
Crossing pedestrian volumes (pedestrians per hour)	100	200	300	100	200	300	100	200	300
Through queue clearing time (s)	3	3	3	3	3	3	3	3	3
Time window for permissive LT (s)	14	30	12	14	30	12	14	30	12
Acceptable gaps for permissive LT (s)	8	8	8	8	8	8	8	8	8
Pedestrian walk time (s)	5	5	5	5	5	5	5	5	5
Pedestrian clearance time (s)	10	10	10	10	10	10	10	10	10

Note: LT = left-turn.

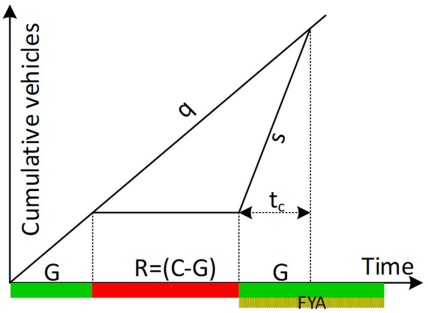

Fig. 4. Queue clearing time calculation with the cumulative counting curves about Westbound (WB) left-turn vehicles (City of Irving, Texas).

During t_c, left-turn vehicles cannot find acceptable gaps. The permissive time window for the left-turn vehicles with a cycle is

$$T = G - t_c = G - \frac{(C-G)}{(\frac{s}{q}-1)} = \frac{(sG-qC)}{(s-q)} \tag{3}$$

Assuming that new opposing through vehicles arrive randomly, then the headway between arrivals can be approximated by an exponential distribution. The cumulative distribution function (CDF) function of the headway h is

$$F_{(h,q)} = \begin{cases} 1-e^{-qh} & h \geq 0 \\ 0 & h < 0 \end{cases} \quad \text{(multiple lanes)} \tag{4a}$$

$$F_{(h,q)} = \begin{cases} 1-e^{-qh} & h \geq h_{\text{safe}} \\ 0 & h < h_{\text{safe}} \end{cases} \quad \text{(single lane)} \tag{4b}$$

From Eqs. (4*a*) and (4*b*), after the queue is cleared, the mean headway in seconds will be $(3{,}600/q)$ s, and the expected number of gaps of opposing through traffic during the permissive left-turn time window will be $T/(3{,}600/q)$. We can also estimate that the probability that headway is equal to or greater than the acceptable gap as follows:

$$F_h\{h > h_a\} = 1-(1-e^{-qh_a}) = e^{-qh_a} \tag{5}$$

So, the maximal left-turn capacity during the permissive time window will be

$$c_{\text{permLT}} = \frac{T}{(\frac{3{,}600}{q})} \times e^{-qh_a} = \frac{(sG-qC)}{(s-q)} \times q \times e^{-qh_a} \tag{6}$$

The average pedestrian arrivals per cycle n_p can be calculated as $n_p = p/(3{,}600/C)$. Only pedestrians arriving during yellow and all-red can activate the pedestrian crossing request and then activate the D-FYA strategy. As a result

$$n_p = \frac{p}{(\frac{3{,}600}{C})}(C-G) \tag{7}$$

When pedestrians are only on the near side or on both sides (Fig. 3), then they will use all the walking and pedestrian clearance time to cross the intersection. During that period, the D-FYA will indicate a red arrow for left-turn vehicles. After the pedestrian clearance timer expires, FYA will be displayed. As such, the remaining permissive time window T' will be

$$T' = T - t_{\text{WALK}} - t_{\text{PC}} = \frac{(sG-qC)}{(s-q)} - t_{\text{WALK}} - t_{\text{PC}} \tag{8}$$

The permissive left-turn saturation flow rate is

$$\frac{T'}{(\frac{1}{q})} \times (1-e^{-qh_a}) = \left(\frac{(sG-qC)}{(s-q)} - t_{\text{WALK}} - t_{\text{PC}}\right) \times q \times e^{-qh_a} \tag{9}$$

When pedestrians are only on the far side, then they will take about 50% of pedestrian clearance time to cross the hazard zone, and then the D-FYA will start the flash yellow arrow for left-turn vehicles. The permissive left-turn capacity in this case is

$$\left(\frac{(sG-qC)}{(s-q)} - t_{\text{WALK}} - \frac{t_{\text{PC}}}{2}\right) \times q \times e^{-qh_a} \tag{10}$$

If $n_p \leq 1$, then the presence probability of one crossing pedestrian with each cycle will be n_p and the pedestrian can appear either on the near side or far side with equal (50%) probabilities (Fig. 3). The expected permissive left-turn saturation flow rate under D-FYA can be estimated as follows:

$$\bar{s}_{\text{permLT}} = \frac{\left(\left(\left(\frac{(sG-qC)}{(s-q)} - t_{\text{WALK}} - t_{\text{PC}}\right) \times q \times e^{-qh_a}\right) + \left(\left(\frac{(sG-qC)}{(s-q)} - t_{\text{WALK}} - \frac{t_{\text{PC}}}{2}\right) \times q \times e^{-qh_a}\right)\right)}{2} \tag{11}$$

If $n_p > 1$, then it can be assumed there is more than one pedestrian every cycle and they can be all on the near side, all on the far side, or both sides with equal (33%) probability.

The expected permissive left-turn saturation flow rate of the D-FYA can be estimated as follows:

$$\bar{s}_{\text{permLT}} = \frac{\left(2 \times \left(\left(\frac{(sG-qC)}{(s-q)} - t_{\text{WALK}} - t_{\text{PC}}\right) \times q \times e^{-qh_a}\right) + \left(\left(\frac{(sG-qC)}{(s-q)} - t_{\text{WALK}} - \frac{t_{\text{PC}}}{2}\right) \times q \times e^{-qh_a}\right)\right)}{3} \tag{12}$$

Fig. 5 shows the permissive left-turn saturation flow rates under different traffic scenarios defined in Table 1.

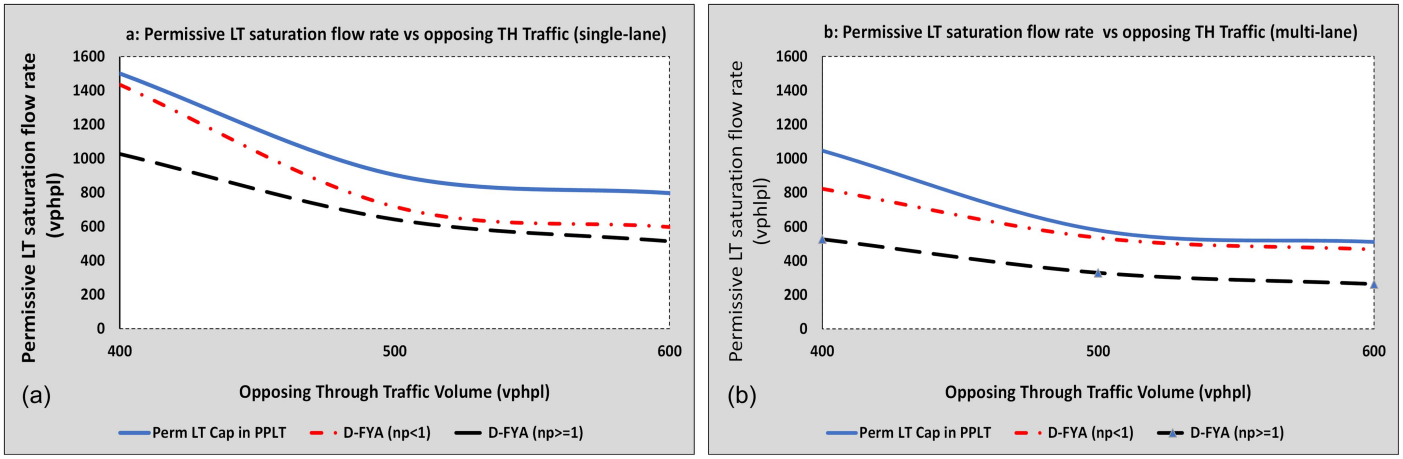

Fig. 5. Sensitivity of permissive (perm) left-turn saturation flow rate under different conditions: (a) permissive LT saturation flow rate versus opposing TH traffic (single-lane); and (b) permissive LT saturation flow rate versus opposing TH traffic (multi-lane).

Discussion

The following points of discussion are highlighted:

- From Eq. (6), if the opposing through traffic volume q is high, the permissive left-turn capacity will be close to zero. In that case, the traffic signal timing should only use a protected left-turn strategy to discharge the left-turn vehicles.
- From Eqs. (11) and (12), if the mainline green is much longer than the walk and pedestrian clearance time or even almost equal to the cycle length, then the D-FYA will reserve significant permissive left-turn capacities while separating the pedestrians from left-turn vehicles. By contrast, the PPLT with minus-pedestrian phase will not reserve any permissive left-turn capability when pedestrians arrive with every cycle.
- The preceding analysis is limited to isolated intersections because it assumes random arrivals of opposing through traffic after the queue is cleared. If an intersection is in coordination, then exponentially distributed headway for new arriving vehicles may be no longer valid because upstream vehicles will arrive in platoons. The analysis of acceptable gaps for coordinated intersections must be empirically performed.
- The permissive left-turn saturation flow rate analysis is grounded on the seminal literature due to Akcelik (1981). The trend of permissive left-turn saturation flow rates under various opposing through traffic volumes is consistent with Akcelik's (1981) model. The research contribution to intersection capacity in this paper is to demonstrate how to extend the classic capacity analysis framework to estimate the permissive left-turn saturation flow rate under modern (i.e., complex) traffic control strategies. In addition, the capacity analysis in this paper also considers the crossing pedestrians and their impact on intersection capacity under actuated traffic control mode.

Case Study I: Evaluation of D-FYA's Performance Using the Emulation-in-the-Field Traffic Signal Simulation Framework

In this experiment, the performance of the proposed D-FYA algorithm in the field is evaluated by verifying its real-time decisions according to the observed pedestrian behaviors in the field. The experiment design is referred to as the emulation-in-the-field framework. It means all the traffic signal inputs and pedestrian behaviors are instantaneously collected in the real world to drive the D-FYA decision making, whereas the D-FYA decisions are not implemented but reported to the observers for verification. The purpose of this experiment is to evaluate the algorithm's reliability and accuracy in the field.

The selected intersection is Cooper Street at UTA Boulevard, a major intersection connecting two urban campuses of the University of Texas at Arlington. The daily pedestrians crossing Cooper Street (mainline) range from 1,000 to 1,500 in a school day. The phasing sequence and pedestrian tracking zones are shown in Fig. 6. There are four flash yellow arrows on all four approaches.

Whenever a phase starts, the D-FYA algorithm will run and report its findings (e.g., the presence of waiting pedestrians) and decisions (e.g., suppressing or activating an FYA) on the console screen. At the same time, a researcher verified the reported decisions according to their observations in the field based on the expected decisions according to the algorithm. The observation was carried out over 100 signal cycles with pedestrian crossings. Table 2 demonstrates how the D-FYA decisions were recorded and verified, using five cycles as an example.

The case study was conducted for 100 cycles in the field. There were 70 cycles where at least one pedestrian phase was called. Among those 70 cycles, 25 cycles only had near-end pedestrians, 25 cases with far-end pedestrians, and nine cases with pedestrians on both sides. Comparing what the D-FYA reported on the screen and what was observed in the field, it is concluded that the D-FYA algorithm could make correct decisions in 93 cycles out of 100 cycles. Table 3 summarizes the D-FYA's performance under various scenarios.

After finishing the experiment in the field, the recorded video and identified possible reasons are further analyzed for incorrect D-FYA decisions. In those failed cases, the pedestrians either leaned on traffic light poles or multiple pedestrians stood too close for the LiDAR tracking algorithm to separate them effectively. This accuracy rate should further increase if the LiDAR tracking algorithm can improve in the future.

Case Study II: Evaluation of the D-FYA Strategy Using the Cabinet-in-the-Loop Traffic Signal Simulation Platform

Mobility Evaluation

The mobility performance of the D-FYA was evaluated as opposed to the other two common permissive left-turn strategies: (1) PPLT;

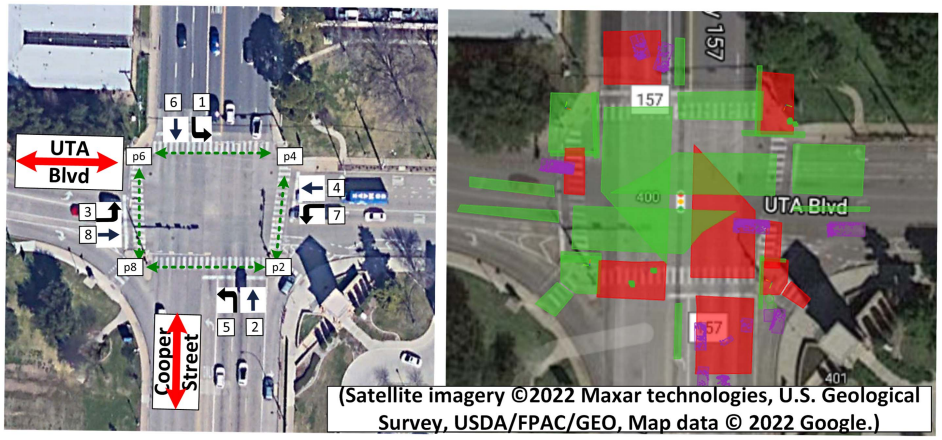

Fig. 6. (a) Phasing sequence; and (b) pedestrian sensing zone layout at Cooper Street at UTA Boulevard, Arlington, Texas. (Satellite imagery ©2022 Maxar technologies, US Geological Survey, USDA/FPAC/GEO, Map data © 2022 Google.)

Table 2. Records of emulation-in-the-field to verify the D-FYA strategy

Signal cycle	Corresponding signal phases	Near-end pedestrians presence	Far-end pedestrian presence	Both ends pedestrians presence	No pedestrians presence	FYA started as scheduled	FYA delayed	FYA canceled	Comment[a]
1	8	1	0	0	0	0	0	1	1
2	4	1	0	0	0	0	1	0	1
3	4	0	0	0	1	1	0	0	2
4	4	1	0	0	0	0	1	0	1
5	4	0	1	0	0	0	1	0	1

[a]In this column, 1 = verified by the researcher in the field, and 2 = verified a pedestrian phase call but no pedestrian presence.

Table 3. Performance summary of D-FYA algorithm under different scenarios

Item	Value
Cycles with no pedestrian calls	30
Cycles only with near-end pedestrians	25
Cycles only with far-end pedestrians	25
Cycles with both-end pedestrians	9
Cycles with pedestrian calls but no pedestrian presence	11
Accuracy rate of the D-FYA algorithm (%)	93

and (2) protected + permissive + minus-pedestrian-phase. The first strategy is to show the left-turn vehicles with a green arrow followed by a flash yellow arrow, whereas the second strategy is to show the left-turn vehicles with a green arrow first and then examine if a pedestrian call is placed. If so, then a red arrow is displayed until the end of the opposing green. Otherwise, the flash yellow arrow is activated.

The intersection of the West Walnut Hill Lane at the North Belt Line Road in the City of Irving, Texas, was selected to develop a simulation model. Fig. 7 shows the movements and phasing sequence.

Cabinet-in-the-Loop Traffic Signal Simulation Platform

The minus-pedestrian-phase feature was not available in traffic signal controllers until very recently. So, it has not yet been supported by any traffic signal simulation engine. To keep a high-fidelity and

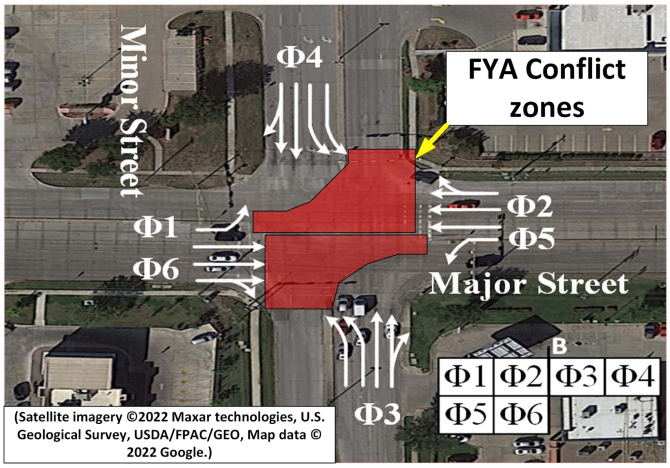

Fig. 7. Layout of intersection for the second case study. (Satellite imagery ©2022 Maxar technologies, US Geological Survey, USDA/FPAC/GEO, Map data © 2022 Google.)

fair comparison, a cabinet-in-the-loop traffic signal simulation platform was developed for this experiment. As shown in Fig. 8, two control units (CUs) are coupled with the VISSIM simulation engine. The first CU is a fully scaled traffic signal assembly. Through the input and out serial ports of the assembly, the latest traffic signal status is retrieved in the traffic signal controller and then sent into VISSIM simulation via the provided traffic signal

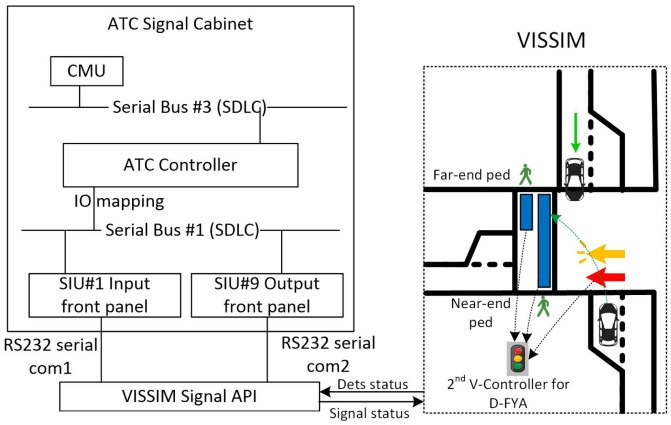

Fig. 8. Architecture of cabinet-in-the-loop traffic signal simulation for the D-FYA evaluation. CMU = cabinet monitor unit; SDLC = synchronous data link control; ATC = advanced traffic controller; IO = input output; and SIU = serial interface unit.

control application programming interface (API). On the other hand, the real-time detector status in the simulation is collected via the signal control API and then sent into traffic signal assembly via its input serial port. The hardware traffic signal controller will decide according to the detector inputs, including the FYA and minus pedestrian phase for the FYA.

A challenge in this experiment is that pedestrian tracking is not straightforward in simulation. To address this issue, a second virtual controller in simulation was developed for the D-FYA strategy. Its logic is to issue a red arrow if there are crossing pedestrians (i.e., the detectors are occupied by pedestrians) otherwise, it will issue a green arrow. The virtual controller issues red light only when the pedestrian phase is activated, so pedestrians (if any) enter the intersection. The simplified D-FYA algorithm will not lose its generality because pedestrians have no random exceptions in a simulation like jaywalking.

As shown in Fig. 8, the detectors are configured to detect concurrent crossing pedestrians. Two signal heads, controlled by the hardware controller and by the virtual D-FYA controller, respectively, are placed in sequence for the left-turn vehicles. The permissive left-turn vehicles can seek gaps and enter only if neither traffic signal head is red. As an illustration, when the opposing (SB in Fig. 8) traffic light turns green with the concurrent pedestrian phase, the hardware traffic signal controller will turn the first signal head to a flash yellow arrow. Meanwhile, if the virtual controller detects the presence of crossing pedestrians, it will turn red, preventing vehicles from entering the intersection. If the virtual controller does not detect the pedestrian presence, it will indicate a green arrow. A flashing yellow arrow and a green arrow will allow left-turn vehicles to enter the intersection during the permissive left-turn phase. This configuration can, in essence, start, delay, or cancel a programmed FYA within a cycle.

Without loss of generality, the mainline vehicle and concurrent crossing pedestrian volumes were set as low, medium, and high to evaluate the performance of three permissive left-turn strategies (Table 4). The experiment also excluded the possibility of starvation by extending the mainline left-turn lanes to ensure the mainline traffic was not affected by different permissive left-turn strategies.

Nine simulation scenarios were generated with the combination of available vehicle and pedestrian volumes. They are referred to as follows:

1. LVLP: low vehicle volumes and low pedestrian volumes.
2. LVMP: low vehicle volumes and medium pedestrian volumes.
3. LVHP: low vehicle volumes and high pedestrian volumes.
4. MVLP: medium vehicle volumes and low pedestrian volumes.
5. MVMP: medium vehicle volumes and medium pedestrian volumes.
6. MVHP: medium vehicle volumes and high pedestrian volumes.
7. HVLP: high vehicle volumes and low pedestrian volumes.
8. HVMP: high vehicle volumes and medium pedestrian volumes.
9. HVHP: high vehicle volumes and high pedestrian volumes.

Fig. 9 shows the mainline left-turn queue length (m) comparison among three permissive left-turn strategies. It reveals that the mobility performance of D-FYA is between the PPLT and PPLT with minus-pedestrian-phase in most cases. In some cases, the D-FYA is much better than the PPLT+minus-pedestrian phase (e.g., the MVHP scenarios) in mobility when separating the left-turn vehicles and pedestrians. When the opposing through traffic and pedestrian volumes are both high, all three permissive left-turn strategies will degrade to the protected-only left-turn strategies (e.g., the HVHP scenario) because the left-turn vehicles cannot find acceptable gaps. A similar pattern is also shown in the delay analysis (Fig. 10).

Discussion

From the simulation results, it can be concluded that for both low vehicle and medium traffic conditions, PPLT and D-FYA had better performance over the PPLT+minus-pedestrian-phase strategy whereas the D-FYA and PPLT with a minus-pedestrian phase have the same pedestrian protection. However, when both vehicle and pedestrian volumes increase to a high level, all three permissive left-turn strategies showed similar delays and queue lengths to the protected-only left-turn strategy. This is because the left-turn vehicles cannot find acceptable gaps during FYA. It implies that any permissive left-turn strategies under certain scenarios might need to be prohibited.

Safety Evaluation

We also studied the performance of D-FYA to decrease traffic conflicts in terms of near misses, average time-to-collision (TTC), and postencroachment time (PET), as opposed to the standard FYA strategies. Using the same simulation platform in the second case, two zones were drawn in the traffic simulation model to collect traffic conflicts relevant to FYA, including the traffic conflicts among, permissive left-turn vehicles, opposing through vehicles,

Table 4. Vehicle and pedestrian volumes for different scenarios

	Southbound			Northbound			Westbound			Eastbound			
Volume	L	T	R	L	T	R	L	T	R	L	T	R	Pedestrians
Low	75	200	30	75	200	30	300	500	120	300	500	130	100
Medium	75	200	30	75	200	30	500	500	120	500	500	130	200
High	75	200	30	75	200	30	750	500	120	750	500	130	350

Note: L = left turn; T = through; and R = right turn.

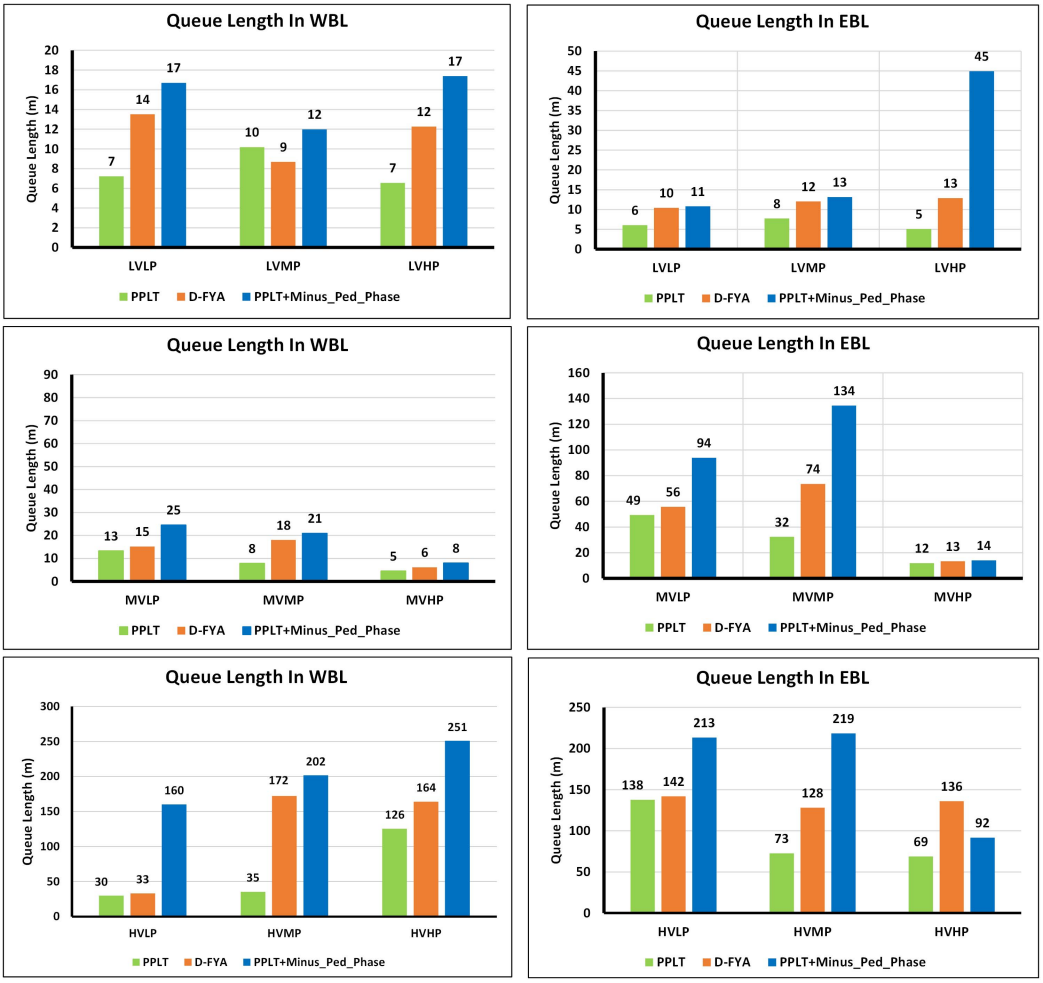

Fig. 9. Mainline left-turn queue length comparison under various scenarios. WBL = westbound left turn; and EBL = eastbound left turn.

and concurrent crossing pedestrians (Fig. 7). The simulation model was then set to output a raw data (*.trj) file for traffic conflict analysis based on safety surrogate assessment model (SSAM) (Pu et al. 2008).

With typical values for max TTC (3 s) and PET (5 s), the raw trajectory files from VISSIM were postprocessed with the open-source SSAM (version 3) provided by the Federal Highway Administration (2017). Each simulation scenario was 60 min with 10 repetitions and different random seeds. The values in Table 5 are an average of 10 runs for each scenario. To simplify, we discard the minus-pedestrian phase feature in the traffic conflict analysis to ensure the difference of traffic conflicts are only caused by standard FYA and D-FYA strategies.

Table 5 indicates that the number of conflicts caused by permissive left turns can be significantly reduced under the D-FYA control strategies, and the differences between mean TTC and PED are not significant under FYA and D-FYA control strategies.

Conclusion and Future Work

In this study, a novel D-FYA mechanism was developed to leverage the permissive left-turn capacity and crossing pedestrians' safety based on pedestrian tracking technologies. The research outcome is to address the reported potential safety hazards after the FYA permissive left-turn strategy is widely deployed. Through a novel emulation-in-the-field traffic signal control framework, the resilience of the proposed D-FYA algorithm to random pedestrian behaviors and mitigations to inaccurate pedestrian detections was verified. Compared with the traditional FYA, the proposed D-FYA based on pedestrian tracking offers four permissive left-turn options for vehicles according to the instantaneous waiting pedestrian's presence at different locations. It provides a highly flexible mechanism to separate the left-turn vehicles from concurrent pedestrians while maximizing the remaining permissive left-turn capacities.

In addition, in a controlled simulation environment, we further evaluated all three permissive left-turn strategies: PPLT, D-FYA, and PPLT with a minus-pedestrian phase. It was concluded that the proposed D-FYA-based pedestrian tracking would be more efficient than the PPLT with a minus-pedestrian phase. At the same time, it can effectively reduce the traffic conflicts related to flashing yellow arrows according to the SSAM. It was also found that when the opposing through traffic became highly, all three permissive left-turn strategies degraded to the protected-only control strategy, leading to high delays and long queues.

In the future, more features can be introduced into the D-FYA strategy, considering the concurrent crossing of pedestrians and the opposing through traffic. As revealed in the experiment, it would be better to dynamically cancel and recover the FYA according to the volume of opposing traffic. It may reduce the possibility of collisions between left-turn vehicles and opposing through vehicles.

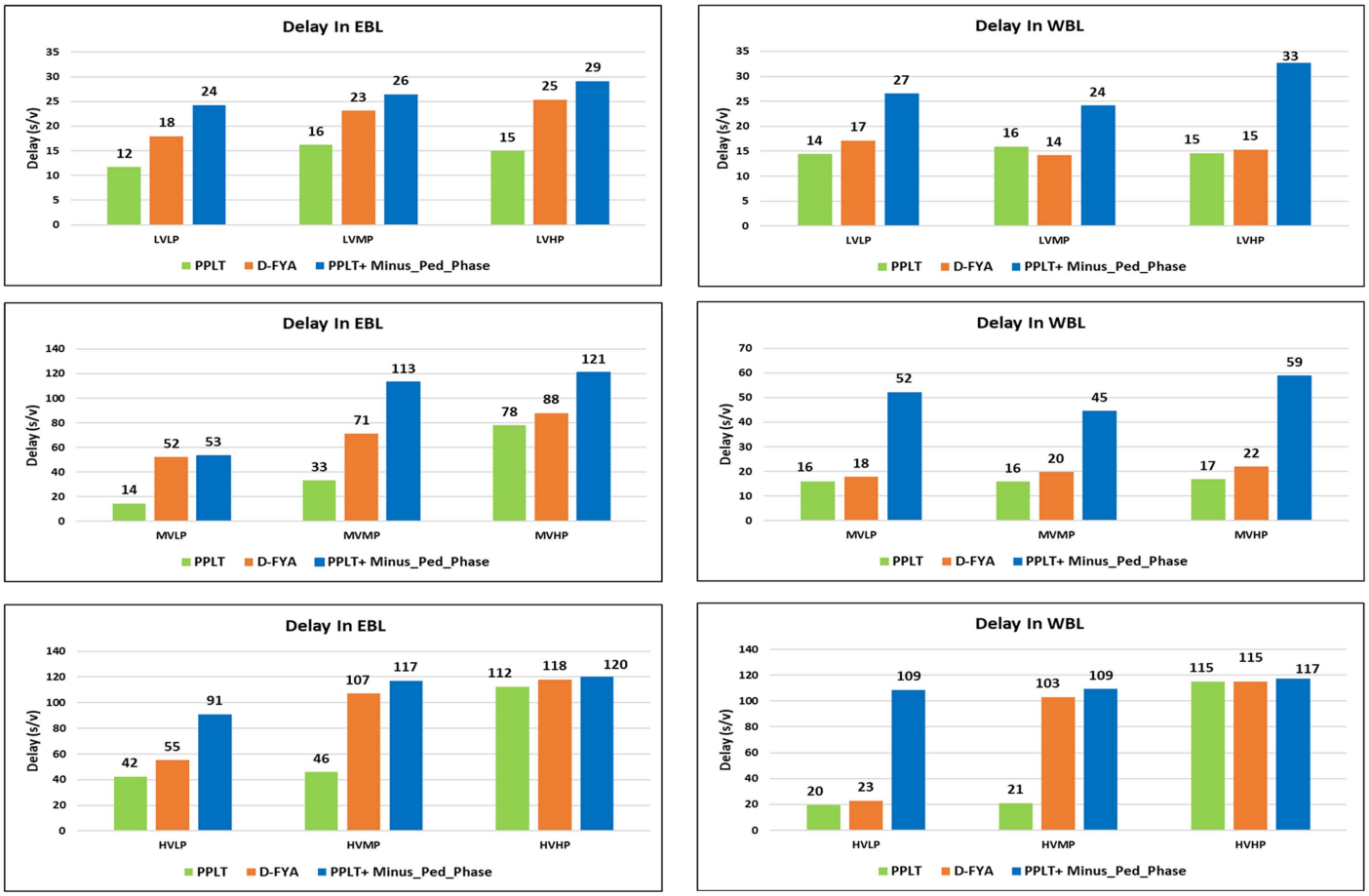

Fig. 10. Mainline left-turn delay comparison under various scenarios. WBL = westbound left turn; and EBL = eastbound left turn.

Table 5. Traffic conflict analysis under different scenarios using SSAM

Traffic volume	Permissive left-turn strategy	Total captured conflicts	Mean TTC	Mean PET
Low	FYA	58	0.27	0.27
Low	D-FYA	36	0.12	0.11
Medium	FYA	718	0.03	0.02
Medium	D-FYA	676	0.07	0.06
High	FYA	860	0.06	0.03
High	D-FYA	730	0.03	0.03

Data Availability Statement

Some or all data, models, or code generated or used during the study are available in a repository online in accordance with funder data retention policies. The simulation model for the second case study can be downloaded at https://github.com/pflee2002/D-FYA-VISSIM-Model.

Acknowledgments

This study is a part of a research project titled *Using LiDAR sensors to study pedestrian behaviors and safety improvement at signalized intersections*, sponsored by the National Institute for Transportation and Communities, a national university transportation center hosted at Portland State University. Any opinions, findings, conclusions, or recommendations expressed in this material are those of the authors. They do not necessarily reflect the official views or policies of the above organizations, nor do the contents constitute a standard, specification, or regulation of these organizations.

Notation

The following symbols are used in this paper:

C = cycle length (s);
c_{permLT} = permissive left turn capability;
G = green duration of opposing through traffic;
h = headway (s);
h_a = acceptable gap for left-turning (s);
h_{safe} = minimal safe headway;
p = volume of concurrent crossing pedestrian (pedestrians per hour);
q = volume of opposing through traffic (vehicles per hour per lane);
s = saturation rate (vehicles per hour per lane);
s_{permLT} = left-turn saturation flow rate during the permissive protected left turn (vehicles per hour per lane);
$\bar{s}_{\text{permLT}}$ = left-turn saturation flow rate during FYA (vehicles per hour per lane);
T = time window for permissive left turn (s);
T' = time window for permissive left-turn under D-FYA (s);
t_c = queue clearing time (s);
t_{pc} = pedestrian clearance time (s); and
t_{walk} = pedestrians walk time (s).

References

Akcelik, R. 1981. *Traffic signals: Capacity and time analysis*. Melbourne, Australia: Australian Road Research Board.

Baek, J., S. Hong, J. Kim, and E. Kim. 2017. "Efficient pedestrian detection at nighttime using a thermal camera." *Sensors* 17 (8): 1850. https://doi.org/10.3390/s17081850.

Bhuvaneshwar, V., and P. B. Mirchandani. 2004. "Real-time detection of crossing pedestrians for traffic-adaptive signal control." In *Proc., 7th Int. IEEE Conf. on Intelligent Transportation Systems (IEEE Cat. No. 04TH8749)*, 309–313. New York: IEEE.

Chan, A. B., Z.-S. J. Liang, and N. Vasconcelos. 2018. "Privacy preserving crowd monitoring: Counting people without people models or tracking." In *Proc., 2008 IEEE Conf. on Computer Vision and Pattern Recognition*, 1–7. New York: IEEE.

Chan, A. B., and N. Vasconcelos. 2009. "Bayesian Poisson regression for crowd counting." In *Proc., 2009 IEEE 12th Int. Conf. on Computer Vision*, 545–551. New York: IEEE.

Combs, T. S., L. S. Sandt, M. P. Clamann, and N. C. McDonald. 2019. "Automated vehicles and pedestrian safety: Exploring the promise and limits of pedestrian detection." *Am. J. Preventive Med.* 56 (1): 1–7. https://doi.org/10.1016/j.amepre.2018.06.024.

El Ansari, M., R. Lahmyed, and A. Trémeau. 2018. "A hybrid pedestrian detection system based on visible images and LIDAR data." In *Proc., VISIGRAPP (5: VISAPP)*, 325–334. Lisboa, Portugal: Institute for Systems and Technologies of Information, Control and Communication.

Federal Highway Administration. 2017. "Safety surrogate assessment module." Accessed November 17, 2016. https://github.com/OSADP/SSAM.

Grassi, A. P., V. Frolov, and F. P. León. 2011. "Information fusion to detect and classify pedestrians using invariant features." *Inf. Fusion* 12 (4): 284–292. https://doi.org/10.1016/j.inffus.2010.06.002.

Gutfreund, O. D. 2004. *Twentieth-century sprawl: Highways and the reshaping of the American landscape*. New York: Oxford University Press.

Islam, M. M., A. A. R. Newaz, and A. Karimoddini. 2021. "A pedestrian detection and tracking framework for autonomous cars: Efficient fusion of camera and Lidar data." In *Proc., 2021 IEEE Int. Conf. on Systems, Man, and Cybernetics (SMC)*, 1287–1292. New York: IEEE.

John, V., S. Tsuchizawa, Z. Liu, and S. Mita. 2017. "Fusion of thermal and visible cameras for the application of pedestrian detection." *Signal Image Video Process.* 11 (3): 517–524. https://doi.org/10.1007/s11760-016-0989-z.

Khalifa, A. B., I. Alouani, M. A. Mahjoub, and N. E. B. Amara. 2020. "Pedestrian detection using a moving camera: A novel framework for foreground detection." *Cognitive Syst. Res.* 60 (May): 77–96. https://doi.org/10.1016/j.cogsys.2019.12.003.

Kilambi, P., E. Ribnick, A. J. Joshi, O. Masoud, and N. Papanikolopoulos. 2008. "Estimating pedestrian counts in groups." *Comput. Vision Image Understanding* 110 (1): 43–59. https://doi.org/10.1016/j.cviu.2007.02.003.

Kim, J. 2019. "Pedestrian detection and distance estimation using thermal camera in night time." In *Proc., 2019 Int. Conf. on Artificial Intelligence in Information and Communication (ICAIIC)*, 463–466. New York: IEEE.

Klein, L. A., M. K. Mills, and D. R. Gibson. 2006. *Traffic detector handbook: Volume I*. McLean, VA: Turner-Fairbank Highway Research Center.

Knodler, M. A., Jr., D. A. Noyce, K. C. Kacir, and C. L. Brehmer. 2007. *An evaluation of driver comprehension of solid yellow indications resulting from implementation of flashing yellow arrow*. Rep. No. 07-2293. Washington, DC: Transportation Research Board.

Kothuri, S., K. Nordback, A. Schrope, T. Phillips, and M. Figliozzi. 2017. "Bicycle and pedestrian counts at signalized intersections using existing infrastructure: Opportunities and challenges." *Transp. Res. Rec.* 2644 (1): 11–18. https://doi.org/10.3141/2644-02.

Levinson, D. M., and K. J. Krizek. 2007. *Planning for place and plexus: Metropolitan land use and transport*. New York: Routledge.

Li, B., Q. Yao, and K. Wang. 2012. "A review on vision-based pedestrian detection in intelligent transportation systems." In *Proc., 9th IEEE Int. Conf. on Networking, Sensing and Control*, 393–398. New York: IEEE.

Lv, B., R. Sun, H. Zhang, H. Xu, and R. Yue. 2019. "Automatic vehicle-pedestrian conflict identification with trajectories of road users extracted from roadside LiDAR sensors using a rule-based method." *IEEE Access* 7 (Nov): 161594–161606. https://doi.org/10.1109/ACCESS.2019.2951763.

Manston, K. 2011. "The challenges of using radar for pedestrian detection." *Traffic Eng. Control* 52 (7): 19–21.

MUTCD (Manual on Uniform Traffic Control Devices). 2009. "Manual on uniform traffic control devices." Accessed December 1, 2009. https://mutcd.fhwa.dot.gov/pdfs/2009/pdf_index.htm.

Noyce, D. A., A. R. Bill, and M. A. Knodler Jr. 2014. *Evaluation of the flashing yellow arrow (FYA) permissive left-turn in shared yellow signal sections*. No. NCHRP Project 20-07/Task 283. Washington, DC: National Academy of Sciences, Engineering, and Medicine.

Pu, L., R. Joshi, and S. Energy. 2008. *Surrogate safety assessment model (SSAM)–Software user manual*. McLean, VA: Turner-Fairbank Highway Research Center.

Q-Free America. 2022. *MaxTime 2.x reference guide*, 461. Carlsbad, CA: Q-Free America.

Soundrapandiyan, R., and P. C. Mouli. 2015. "Adaptive pedestrian detection in infrared images using background subtraction and local thresholding." *Procedia Comput. Sci.* 58 (1): 706–713. https://doi.org/10.1016/j.procs.2015.08.091.

Tang, S., M. Ye, C. Zhu, and Y. Liu. 2017. "Adaptive pedestrian detection using convolutional neural network with dynamically adjusted classifier." *J. Electron. Imaging* 26 (1): 013012. https://doi.org/10.1117/1.JEI.26.1.013012.

Tarko, A. 2019. *Measuring road safety with surrogate events*. Amsterdam, Netherlands: Elsevier.

Wu, J., H. Xu, Y. Sun, J. Zheng, and R. Yue. 2018. "Automatic background filtering method for roadside LiDAR data." *Transp. Res. Rec.* 2672 (45): 106–114. https://doi.org/10.1177/0361198118775841.

Yan, Y., M. Xu, J. S. Smith, M. Shen, and J. J. P. R. Xi. 2021. "Multicamera pedestrian detection using logic minimization." *Pattern Recognit.* 112 (Apr): 107703. https://doi.org/10.1016/j.patcog.2020.107703.

Yang, H., Y. Zhang, Y. Zhang, H. Meng, S. Li, and X. Dai. 2021. "A fast vehicle counting and traffic volume estimation method based on convolutional neural network." *IEEE Access* 9 (Nov): 150522–150531. https://doi.org/10.1109/ACCESS.2021.3124675.

Yoshinaga, S., A. Shimada, and R.-i. Taniguchi. 2010. "Real-time people counting using blob descriptor." *Procedia-Social Behav. Sci.* 2 (1): 143–152. https://doi.org/10.1016/j.sbspro.2010.01.028.

Zhao, H., J. Sha, Y. Zhao, J. Xi, J. Cui, H. Zha, and R. Shibasaki. 2011. "Detection and tracking of moving objects at intersections using a network of laser scanners." *IEEE Trans. Intell. Transp. Syst.* 13 (2): 655–670. https://doi.org/10.1109/TITS.2011.2175218.

Zhao, H., and R. Shibasaki. 2005. "A novel system for tracking pedestrians using multiple single-row laser-range scanners." *IEEE Trans. Syst. Man Cybern. Part A Syst. Hum.* 35 (2): 283–291. https://doi.org/10.1109/TSMCA.2005.843396.

Zhao, J., Y. Li, H. Xu, and H. Liu. 2019. "Probabilistic prediction of pedestrian crossing intention using roadside LiDAR data." *IEEE Access* 7 (Jul): 93781–93790. https://doi.org/10.1109/ACCESS.2019.2927889.

Ziebarth, M. 2020. "NY v. national highway traffic safety admin., 974 F. 3d 87 (2d Cir. 2020)." *Transp. LJ* 47 (Aug): 87.